Excitation of terahertz modes localized on a layered superconductor: Anomalous dispersion and resonant transmission

S. S. Apostolov,[1,2] N. M. Makarov,[1,3,*] and V. A. Yampol'skii[1,2,†]
[1]*A. Ya. Usikov Institute for Radiophysics and Electronics NASU, 61085 Kharkov, Ukraine*
[2]*V. N. Karazin Kharkov National University, 61077 Kharkov, Ukraine*
[3]*Benemérita Universidad Autónoma de Puebla, Puebla, Pue. 72000, México*

(Received 6 November 2017; published 17 January 2018)

We study theoretically the optic transmission through a slab of layered superconductor separated from two dielectric leads by spatial gaps. Based on the transfer matrix formalism along with the Josephson plasma electrodynamic approach, we derive analytic expressions for the transmittance and identify the conditions for the perfect transmission. The special interest of the study is focused on the resonant transmission, which occurs when the wave does not propagate in the spatial gaps. Far from the resonance, the transmittance is exponentially small due to the total internal reflection from the lead-gap interface. However, the excitation of electromagnetic modes localized on the layered superconductor gives rise to a remarkable resonant enhancement of the transmission. Moreover, this phenomenon is significantly modified for the layered superconductors in comparison with usual dielectrics or conductors. The dispersion curves for the modes localized on the layered superconductor are proved to be nonmonotonic, thus resulting in the specific dependence of the transmittance T on the incidence angle θ. In particular, we predict the onset of two resonant peaks in the $T(\theta)$ dependence and their subsequent merge into the broadened single peak with increasing of the wave frequency. Our analytical results are demonstrated by numerical data.

DOI: 10.1103/PhysRevB.97.024510

I. INTRODUCTION

Metamaterials attract considerable attention because of their unusual interaction with electromagnetic waves (see, e.g., Refs. [1–3]). In particular, metamaterials supporting the negative refractive index have the potential for subwavelength resolution [4] and aberration-free imaging. In this relation, the paper [1] of Veselago is often considered as an initial point in the study of the negative refraction. However, the understanding of the essence of this phenomenon was earlier achieved by Mandelstam [5] in the 1940s.

The first proposed metamaterials with negative refractive index used subwavelength electric and magnetic structures to achieve simultaneously negative permittivity ε and permeability μ (see, e.g., Refs. [6,7]). Another promising way to create metamaterials is to construct strongly anisotropic media; in particular, uniaxial anisotropic materials with different signs of the components of permittivity tensor (the so-called hyperbolic metamaterials [8–11]). In Refs. [12–15], it was shown that the high-temperature superconductors can be used as such materials. Indeed, the crystals $Bi_2Sr_2CaCu_2O_{8+\delta}$ and $YBa_2Cu_3O_{7-\delta}$ are characterized by the strong current-carrying anisotropy, i.e., the longitudinal ε_{ab} and transverse ε_c components of the effective permittivity tensor in such media have different signs in a wide frequency range, giving rise to a negative refraction and an anomalous dispersion of the electromagnetic waves.

Experimental studies [16,17] of the conductivity in the layered superconductor structures have elucidated that the superconducting layers are electrodynamically coupled there due to the internal Josephson effect. In such a strongly anisotropic plasma, electromagnetic excitations, called the Josephson plasma waves, arise at the frequencies in the THz range, which is important for the various applications in physics, chemistry, astronomy, security systems, medical diagnostics, and environmental control (see, for example, reviews [18,19] and links inside).

The layered superconductors, such as $Bi_2Sr_2CaCu_2O_{8+\delta}$, have been extensively studied in relation to absorption [20–23] and emission [24–27] of the electromagnetic radiation, especially in the presence of the applied magnetic field. In particular, they are emerging as compact sources of electromagnetic radiation in the sub-THz and THz frequency ranges. The THz emission from the layered superconductors occurs at frequencies above the Josephson plasma frequency ω_J, and recently there has been a breakthrough in that field, when the upper limit of the emission frequency has been raised to 2.4 THz [28], and then to nearly 11 THz [29]. It should be noted that, in the present study, we examine neither absorption nor emission of the radiation, but the wave transport phenomena induced by the internal excitation of the localized Josephson plasma waves.

The interface between a layered superconductor and the vacuum supports the propagation of the surface Josephson plasma waves [13–15], similarly to what happens in the case of usual plasma. However, in contrast to the latter, the surface Josephson plasma waves propagate with the frequencies which can be both lower and higher than the characteristic for

*makarov.n@gmail.com
†yam@ire.kharkov.ua

the layered superconductor frequency, which is called the Josephson plasma frequency [13].

A slab of layered superconductor can also provide the propagation of the THz waves localized on it. We call them waveguide or surface modes depending on whether the electromagnetic field of these waves oscillates or decays across the slab. Recently, the spectrum of such waves has been theoretically studied in two geometries, when the superconducting layers are parallel [30] or perpendicular [31] to the interfaces of the slab. Remarkably, in the second geometry, the dispersion curves of the localized modes appear to be nonmonotonic for some values of the parameters.

In the present paper, we study theoretically the wave propagation through a slab of layered superconductor surrounded by two dielectrics for the geometry when the superconducting layers are perpendicular to the slab boundaries. The main attention is focused on the resonant transmission accompanied by the excitation of the localized modes. It should be emphasized that the particular interest for studying this phenomenon in structures including the layered superconductors is caused by two reasons. First, the characteristic frequencies for observation of the resonant transmission through the layered superconductor belong to the THz range, very important for possible applications. In particular, one could employ the studying resonant phenomenon as a method to tune the emission or receiver frequency from THz sources. Second, this phenomenon is significantly modified for the layered superconductors in comparison with usual dielectrics or conductors. The dispersion curves for the modes localized on the layered superconductor are proved to be nonmonotonic. This results in the specific dependence of the transmittance T on the incidence angle θ. In particular, we predict a merge of two resonant peaks in the $T(\theta)$ dependence with the formation of the broadened single peak, when increasing the wave frequency ω.

The paper is organized as follows. In the second section, we formulate the problem, present the system geometry, and introduce the basic definitions and notations. In the third section, we use the transfer matrix method to describe the electromagnetic waves transfer through the system. The fourth section is devoted to the derivation of the dispersion relation for the localized modes and its analysis. The fifth, sixth, and seventh sections are devoted to the detailed analysis of the transmittance. The fifth section presents the general expressions for the transmittance. In the sixth section, we analyze the resonant transmission and its features due to the nonmonotonic dispersion law for the localized modes. The seventh section contains the numerical simulation of the transmittance with account for the dissipation of the waves in layered superconductors.

II. MODEL FORMULATION

We examine the propagation of an electromagnetic wave through a slab of layered superconductor consisting of alternating dielectric and superconductor layers which are arranged orthogonally to the slab surfaces. The propagation should be provided by the excitation of waveguide/surface modes localized on the slab. To accomplish this purpose we consider the following setup, see Fig. 1.

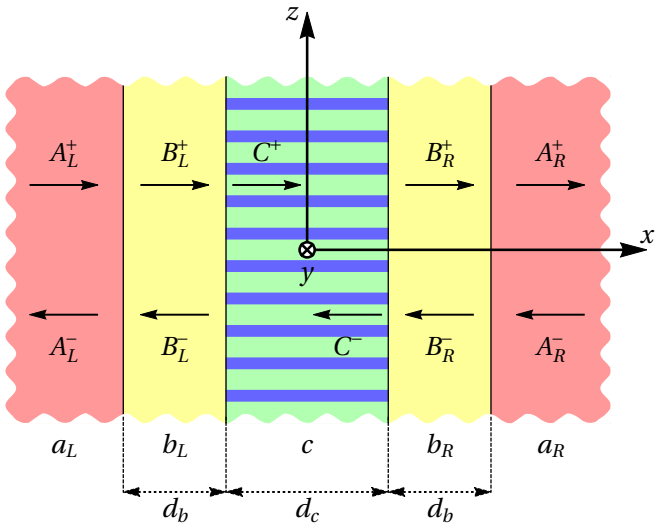

FIG. 1. A sketch of the setup.

The slab c of layered superconductor of thickness d_c is sandwiched between two dielectrics, the left a_L and the right a_R leads (semi-infinite media characterized by the perfect wave transmission) with permittivity ε_a. Two spatial b gaps, b_L and b_R, between c slab and a leads of the same thicknesses d_b are filled with the dielectric of permittivity ε_b. Both the a leads and the spatial b gaps are assumed to be made from the lossless materials, i.e., the values of ε_a and ε_b are real and positive. Note that in the experiment the vacuum with $\varepsilon_b = 1$ can properly serve as a filling material for the spatial b gaps. However, we shall keep the notation ε_b in our theoretical results to extend their applicability. The a leads are assumed to be optically denser than the b gaps, i.e.,

$$\varepsilon_b < \varepsilon_a. \tag{1}$$

This assumption provides the possibility to generate the localized modes by the incident wave (see Sec. IV) which propagates in the a leads and evanesces in the spatial b gaps.

The coordinate system is chosen in such a way that the x axis is orthogonal to all the interfaces of the setup that are parallel to the (y,z) plane; the z axis is orthogonal to the superconductor layers.

The resonant transmission phenomenon analyzed here can be observed only for the electromagnetic waves of TM polarization (or, the same, of p polarization). In view of the chosen coordinate system, this fact implies the following presentation for the components of electric $\vec{E}(x,z,t)$ and magnetic $\vec{H}(x,z,t)$ fields:

$$\vec{E}(x,z,t) = \{E_x(x),0,E_z(x)\}\exp(-i\omega t + ik_z z), \tag{2a}$$

$$\vec{H}(x,z,t) = \{0,H_y(x),0\}\exp(-i\omega t + ik_z z). \tag{2b}$$

Here ω is the wave frequency and k_z is the z projection of the wave vector. These two physical quantities are free external parameters of the problem. However, the perfect wave propagation in the a leads means that

$$k_z < k_0\sqrt{\varepsilon_a}, \quad k_0 = \omega/c. \tag{3}$$

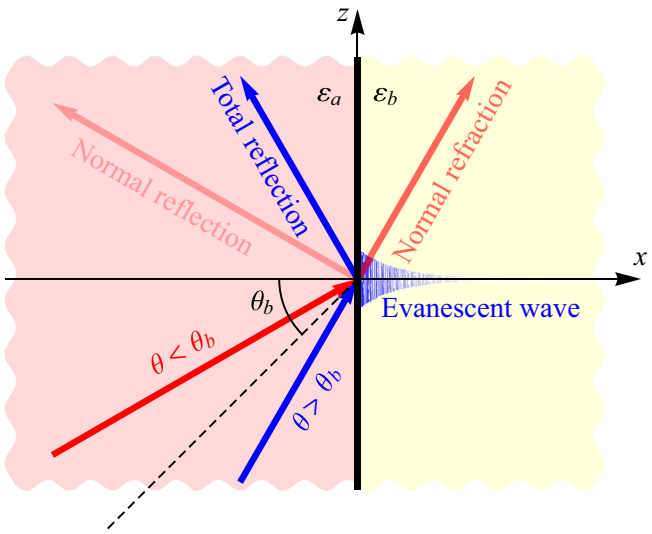

FIG. 2. A schematic diagram for the wave reflection at the interface between semi-infinite dielectric media a and b.

Then, in the case of oblique wave incidence onto the structure interfaces, due to restriction (3), it is reasonable to represent the wave number k_z via the angle θ of incidence of the wave from the a_L lead onto the $(a_L|b_L)$ interface,

$$k_z = k_0\sqrt{\varepsilon_a}\sin\theta, \quad 0 < \theta < \pi/2. \tag{4}$$

In addition, in view of the obligatory condition (1), it is proper to introduce the characteristic incidence angle θ_b,

$$\sin\theta_b = \sqrt{\varepsilon_b/\varepsilon_a}, \quad 0 < \theta_b < \pi/2. \tag{5}$$

This angle is commonly regarded as the limit angle for total internal reflection from the interface between semi-infinite a and b dielectrics. Figure 2 demonstrates schematically the reflection of the waves at this interface. The wave incident at the angle $\theta < \theta_b$ from dielectric a partially reflects into dielectric a and partially refracts into dielectric b. The wave incident at the angle $\theta > \theta_b$ from dielectric a totally reflects into dielectric a and produces the evanescent wave in dielectric b.

In what follows, we consider only the grazing incidence of the wave when

$$k_0\sqrt{\varepsilon_b} < k_z < k_0\sqrt{\varepsilon_a} \to \theta_b < \theta < \pi/2. \tag{6}$$

Due to this constitutive condition, the electromagnetic radiation evanesces in the spatial b gaps, and, therefore, the total internal reflection should be observed at the $(a_L|b_L)$ and $(a_R|b_R)$ interfaces between lead and gap. However, as shown in Sec. V, even in such a case, the excitation of the modes localized on the c slab of the layered superconductor causes perfect transmission for certain values of the problem parameters.

Within the indispensable range (6), the x projection k_a of the wave vector in the a leads is evidently real valued,

$$k_a = \sqrt{k_0^2\varepsilon_a - k_z^2} = k_0\sqrt{\varepsilon_a}\cos\theta. \tag{7}$$

In contrast to the wave number k_a, the x projection k_b of the wave vector in the spatial b gaps turns out to be imaginary due to the left inequality in assumption (6),

$$k_b = i\kappa_b, \quad \kappa_b = \sqrt{k_z^2 - k_0^2\varepsilon_b} = k_0\sqrt{\varepsilon_a}\sqrt{\sin^2\theta - \sin^2\theta_b}\,. \tag{8}$$

The electromagnetic field inside the layered superconductor c is governed by the gauge-invariant phase difference of the order parameter in neighboring superconducting layers. This phase difference obeys the set of coupled sine-Gordon equations (see, e.g., review [18], and references therein). Nevertheless, for the linear waves within the continual approximation, where $k_z d \ll 1$, this phase difference can be excluded from the electrodynamic equations. As a consequence, the problem is reformulated in terms of an anisotropic frequency-dispersive permittivity tensor with in-plane and out-of-plane components [12],

$$\varepsilon_{xx}(\omega) = \varepsilon_{yy}(\omega) = \varepsilon_c\left(1 - \gamma^2\frac{\omega_J^2}{\omega^2} + i\nu_x\frac{\omega_J}{\omega}\right), \tag{9a}$$

$$\varepsilon_{zz}(\omega) = \varepsilon_c\left(1 - \frac{\omega_J^2}{\omega^2} + i\nu_z\frac{\omega_J}{\omega}\right), \tag{9b}$$

respectively. Here $\omega_J = (8\pi e j_c d/\hbar\varepsilon_c)^{1/2}$ is the Josephson plasma frequency, j_c is the maximal Josephson current density, ε_c and d are the positive permittivity and the thickness of the insulator layers, and e is the elementary charge. The dimensionless relaxation frequencies $\nu_{x,z} = 4\pi\sigma_{x,z}/\varepsilon_c\omega_J$ are proportional to the averaged quasiparticle conductivities along, σ_x, and across, σ_z, the superconducting layers. The London penetration depth along the layers, $\lambda_c = c/\omega_J\varepsilon_c^{1/2}$, appears to be much greater than that across the layers, λ_{ab}, resulting in the great current-anisotropy parameter $\gamma = \lambda_c/\lambda_{ab} \gg 1$.

The effective wave number k_c which is responsible for the propagation of the TM-polarized electromagnetic field (2) along the x axis through the c slab with the anisotropic permittivity tensor (9), reads

$$k_c = \sqrt{\frac{\varepsilon_{zz}}{\varepsilon_{xx}}}\sqrt{k_0^2\varepsilon_{xx} - k_z^2} = k_0\sqrt{\frac{\varepsilon_{zz}}{\varepsilon_{xx}}\varepsilon_a}\sqrt{\frac{\varepsilon_{xx}}{\varepsilon_a} - \sin^2\theta}. \tag{10}$$

Note that, in general, the permittivities, ε_a of the dielectric a leads and ε_{xx} of the c slab of layered superconductor, can be in arbitrary relation depending on the problem parameters. This fact, together with the specific anisotropic frequency dependence in Eqs. (9), results in a quite sophisticated dependence of k_c on ω and θ (wave number k_z). Now we assume the absence of dissipation, $\nu_x = \nu_z = 0$, and provide a brief analysis of k_c within different frequency ranges.

Inside the low frequency range, $\omega < \omega_J \ll \gamma\omega_J$, all the components of the permittivity tensor (9) are negative, $\varepsilon_{xx} = \varepsilon_{yy} < 0$ and $\varepsilon_{zz} < 0$. Therefore, k_c is imaginary and its absolute value increases with the wave number k_z, i.e., with the incidence angle θ.

In the intermediate frequency range, $\omega_J < \omega < \gamma\omega_J$, the components of the permittivity tensor (9) have different signs, $\varepsilon_{xx} = \varepsilon_{yy} < 0$ and $\varepsilon_{zz} > 0$. Inside this range, the iso-frequency surface in the k space for the Josephson plasma waves has

a hyperboloidal shape, i.e., the layered superconductor represents the so-called hyperbolic medium. Hence, k_c is real valued and increases with the wave number k_z (with the incidence angle θ). It should be emphasized that this nontrivial $k_c(k_z)$, or $k_c(\theta)$, dependence provides the interesting and uncommon wave properties of the layered superconductor, in particular, the anomalous dispersion of the localized modes (see Sec. IV).

Within the high frequency range, $\omega_J \ll \gamma\omega_J < \omega$, all the components of the permittivity tensor (9) are positive, $\varepsilon_{xx} = \varepsilon_{yy} > 0$ and $\varepsilon_{zz} > 0$. The value of k_c can be either real or imaginary depending on k_z^2. However, in the experiment, the high frequency range is hardly attained because of Cooper pairs destroying. Moreover, there is no emission of the electromagnetic wave for the sufficiently high frequencies $\omega > 2\Delta/\hbar$, where Δ is the superconducting energy gap, which are recently [29] restricted as approximately 11 THz for $Bi_2Sr_2CaCu_2O_{8+\delta}$. Therefore, we do not consider the high frequency range in the rest of the paper.

III. TRANSFER MATRIX RELATIONS

Within every a lead, every spatial b gap, as well as inside the c slab of layered superconductor, the magnetic field $H_y(x)$ of the propagating electromagnetic TM wave (2) obeys the 1D Helmholtz equation with corresponding squared wave number, k_a^2, k_b^2, or k_c^2. Its general solution inside the setup constituents can be presented as a superposition of two plane waves traveling in opposite directions (see, e.g., Ref. [32]). By combining these solutions with boundary conditions at the corresponding interfaces, one can obtain the matrix relation that describes the wave transfer through the whole structure,

$$\begin{pmatrix} A_R^+ \\ A_R^- \end{pmatrix} = \hat{M}^{(T)} \begin{pmatrix} A_L^+ \\ A_L^- \end{pmatrix}, \tag{11a}$$

$$\hat{M}^{(T)} = \hat{M}^{(ab)^{-1}} \hat{M}^{(b)} \hat{\mathcal{D}} \hat{M}^{(b)} \hat{M}^{(ab)}. \tag{11b}$$

This relation transforms the amplitudes of incident A_L^+ and reflected A_L^- waves at the left side of the $(a_L|b_L)$ interface into the amplitudes of incident A_R^- and reflected A_R^+ waves at the right side of the $(b_R|a_R)$ interface, see Fig. 1.

Matrix $\hat{M}^{(ab)}$ describes the wave transfer through the $(a_L|b_L)$ interface from the left a_L lead into the left spatial b_L gap. It is defined by

$$\hat{M}^{(ab)} = \frac{1}{2} \begin{pmatrix} 1 + \dfrac{k_a\varepsilon_b}{k_b\varepsilon_a} & 1 - \dfrac{k_a\varepsilon_b}{k_b\varepsilon_a} \\ 1 - \dfrac{k_a\varepsilon_b}{k_b\varepsilon_a} & 1 + \dfrac{k_a\varepsilon_b}{k_b\varepsilon_a} \end{pmatrix}. \tag{12}$$

The inverse matrix $\hat{M}^{(ab)^{-1}}$ correspondingly reads

$$\hat{M}^{(ab)^{-1}} = \frac{1}{2} \begin{pmatrix} 1 + \dfrac{k_b\varepsilon_a}{k_a\varepsilon_b} & 1 - \dfrac{k_b\varepsilon_a}{k_a\varepsilon_b} \\ 1 - \dfrac{k_b\varepsilon_a}{k_a\varepsilon_b} & 1 + \dfrac{k_b\varepsilon_a}{k_a\varepsilon_b} \end{pmatrix}. \tag{13}$$

Note that deriving the inverse matrix (13) is equivalent to mutual (reciprocal) replacement of the indices in the initial matrix (12), i.e., $\hat{M}^{(ab)^{-1}} = \hat{M}^{(ba)}$. It describes the wave transfer through the $(b_R|a_R)$ interface from the right spatial b_R gap into the right a_R lead. The determinants of the matrices are

$$\det \hat{M}^{(ab)} = \frac{k_a\varepsilon_b}{k_b\varepsilon_a}, \quad \det \hat{M}^{(ab)^{-1}} = \frac{k_b\varepsilon_a}{k_a\varepsilon_b}. \tag{14}$$

The diagonal unimodular matrix $\hat{M}^{(b)}$ is responsible for the free wave transfer within the spatial b gaps, specifically, from the right side of the $(a_L|b_L)$ interface up to the left side of the $(b_L|c)$ interface and/or from the right side of the $(c|b_R)$ interface up to the left side of the $(b_R|a_R)$ interface,

$$\hat{M}^{(b)} = \begin{pmatrix} \exp(i\varphi_b) & 0 \\ 0 & \exp(-i\varphi_b) \end{pmatrix}, \quad \det \hat{M}^{(b)} = 1. \tag{15}$$

Therefore, its diagonal elements are just the exponents containing the phase shift $\varphi_b = k_b d_b$ gained by the wave when passing each of the spatial b gaps of the thickness d_b. In accordance with Eqs. (8) for the wave number k_b, the value of φ_b is imaginary,

$$\varphi_b = i\phi_b, \quad \phi_b = d_b\sqrt{k_z^2 - k_0^2\varepsilon_b} = k_0 d_b \sqrt{\varepsilon_a}\sqrt{\sin^2\theta - \sin^2\theta_b}\,. \tag{16}$$

It should be emphasized that Eq. (11b) contains two mutually inverse matrices $\hat{M}^{(ab)}$ and $\hat{M}^{(ba)} = \hat{M}^{(ab)^{-1}}$ and two equal matrices $\hat{M}^{(b)}$. The difference in usage is related to the nature of these matrices. The first two matrices, $\hat{M}^{(ab)}$ and $\hat{M}^{(ba)}$, describe the wave transfer through interfaces $(a_L|b_L)$ and $(b_R|a_R)$, respectively. Since the interfaces are symmetrical, these matrices are mutually inverse. On the contrary, the other two matrices $\hat{M}^{(b)}$ describe the free wave transfer through the identical spatial b gaps. Passing each b gap, the wave gains the same phase shift φ_b and, therefore, two matrices $\hat{M}^{(b)}$ are equal, but not inverse. Nevertheless, these two matrices $\hat{M}^{(b)}$ do not break the symmetry because their determinants are equal to 1, see Eq. (15).

The transfer matrix $\hat{\mathcal{D}}$ for the c slab of layered superconductor is a product of three matrices,

$$\hat{\mathcal{D}} = \hat{M}^{(bc)^{-1}} \hat{M}^{(c)} \hat{M}^{(bc)}. \tag{17}$$

The matrices $\hat{M}^{(bc)}$ and $\hat{M}^{(bc)^{-1}}$ determine the wave transfer via the interface $(b_L|c)$ from the spatial b_L gap into the c slab and via the interface $(c|b_R)$ from the c slab into the adjacent spatial b_R gap, respectively. They have a structure similar to that of the interface-transfer matrices $\hat{M}^{(ab)}$ and $\hat{M}^{(ab)^{-1}}$, and can be readily obtained from Eqs. (12) and (13) by the replacement $k_a\varepsilon_b \to k_b\varepsilon_{zz}$ and $k_b\varepsilon_a \to k_c\varepsilon_b$. Evidently, $\hat{M}^{(bc)^{-1}} = \hat{M}^{(cb)}$. The diagonal matrix $\hat{M}^{(c)}$ corresponds to free wave flight from the left-hand to the right-hand boundary inside the c slab. Therefore, it differs from the matrix $\hat{M}^{(b)}$ only in the wave phase shift. Specifically, Eq. (15) is transformed into the expression for $\hat{M}^{(c)}$ by writing φ_c instead of φ_b,

$$\varphi_c = k_c d_c. \tag{18}$$

By direct multiplication of the matrices, it can be shown that the c slab transfer matrix $\hat{\mathcal{D}}$ has the following elements:

$$\mathcal{D}_{11} = \cos\varphi_c - \alpha_+ \sin\varphi_c, \tag{19a}$$

$$\mathcal{D}_{12} = \alpha_- \sin\varphi_c, \tag{19b}$$

$$\mathcal{D}_{21} = -\alpha_- \sin\varphi_c, \tag{19c}$$

$$\mathcal{D}_{22} = \cos\varphi_c + \alpha_+ \sin\varphi_c. \tag{19d}$$

Here the mismatching factors $\alpha_\pm$ measuring the coupling of the c slab to the spatial b gaps, are defined by

$$\alpha_\pm = \frac{1}{2}\left(\frac{\kappa_b\varepsilon_{zz}}{k_c\varepsilon_b} \mp \frac{k_c\varepsilon_b}{\kappa_b\varepsilon_{zz}}\right), \quad \alpha_-^2 - \alpha_+^2 = 1\,. \tag{20}$$

Note that the determinant of the matrix $\hat{\mathcal{D}}$, as well as the determinant of the total transfer matrix $\hat{M}^{(T)}$, are equal to one due to the general condition inherent for transfer matrices of the systems with symmetric leads,

$$\det\hat{\mathcal{D}} = \mathcal{D}_{11}\mathcal{D}_{22} - \mathcal{D}_{12}\mathcal{D}_{21} = 1, \tag{21a}$$

$$\det\hat{M}^{(T)} = M_{11}^{(T)}M_{22}^{(T)} - M_{12}^{(T)}M_{21}^{(T)} = 1. \tag{21b}$$

Combining Eqs. (11b), (12), (13), and (15), one gets the explicit expressions for the elements of the total transfer matrix $M^{(T)}$,

$$2M_{11}^{(T)} = \left(\mathcal{D}_{11}\mathrm{e}^{-2\phi_b} + \mathcal{D}_{22}\mathrm{e}^{2\phi_b}\right) - i\beta_+\left(\mathcal{D}_{11}\mathrm{e}^{-2\phi_b} - \mathcal{D}_{22}\mathrm{e}^{2\phi_b}\right) + 2i\beta_-\mathcal{D}_{12}, \tag{22a}$$

$$2M_{12}^{(T)} = -2i\beta_+\mathcal{D}_{12} + i\beta_-\left(\mathcal{D}_{11}\mathrm{e}^{-2\phi_b} - \mathcal{D}_{22}\mathrm{e}^{2\phi_b}\right), \tag{22b}$$

$$2M_{21}^{(T)} = 2i\beta_+\mathcal{D}_{12} - i\beta_-\left(\mathcal{D}_{11}\mathrm{e}^{-2\phi_b} - \mathcal{D}_{22}\mathrm{e}^{2\phi_b}\right), \tag{22c}$$

$$2M_{22}^{(T)} = \left(\mathcal{D}_{11}\mathrm{e}^{-2\phi_b} + \mathcal{D}_{22}\mathrm{e}^{2\phi_b}\right) + i\beta_+\left(\mathcal{D}_{11}\mathrm{e}^{-2\phi_b} - \mathcal{D}_{22}\mathrm{e}^{2\phi_b}\right) - 2i\beta_-\mathcal{D}_{12}. \tag{22d}$$

The other mismatching factors, $\beta_\pm$, are real valued due to the basic condition (6) and specify the coupling of the spatial b gaps to the a leads,

$$\beta_\pm = \frac{1}{2}\left(\frac{k_a\varepsilon_b}{\kappa_b\varepsilon_a} \mp \frac{\kappa_b\varepsilon_a}{k_a\varepsilon_b}\right). \tag{23a}$$

It is important to note that within the representation of the independent external parameters ω and θ, the mismatching factors $\beta_\pm$ do not depend on the wave frequency ω, being governed by the incidence angle θ and characteristic angle θ_b,

$$\beta_\pm = \frac{1}{2}\left(\frac{\sin^2\theta_b\cos\theta}{\sqrt{\sin^2\theta - \sin^2\theta_b}} \mp \frac{\sqrt{\sin^2\theta - \sin^2\theta_b}}{\sin^2\theta_b\cos\theta}\right),$$

$$\beta_-^2 - \beta_+^2 = 1\,. \tag{23b}$$

IV. LOCALIZED EIGENMODES

A basic concept of our study is the generation of specific, localized on the slab of layered superconductor, electromagnetic modes due to which a significant enhancement of the transmission can be achieved. In general (see, e.g., book [33]), such excitations belong to the family of the eigenmodes in the systems consisting of a dielectric (or conductor) slab embedded in the infinite medium of softer optical density.

In order to elucidate the features of the localized modes in our setup, consider the truncated system including the c slab imposed between only the left and right spatial b gaps with infinite thicknesses, $d_b \to \infty$ (the a leads are absent). The wave transfer through such a system can be described by the relation that connects the amplitudes of incoming B_L^+ and outgoing B_L^- waves at the left side of the $(b_L|c)$ interface with the amplitudes of outgoing B_R^+ and incoming B_R^- waves at the right side of the $(c|b_R)$ interface, see Fig. 1. As follows from Eq. (11b), the desired transfer relation reads

$$\begin{pmatrix} B_R^+ \\ B_R^- \end{pmatrix} = \hat{\mathcal{D}}\begin{pmatrix} B_L^+ \\ B_L^- \end{pmatrix}. \tag{24}$$

The localization of electromagnetic mode on the c slab of layered superconductor implies a satisfaction of two conditions. First, the mode outside the c slab, i.e., inside both of the spatial b gaps, must contain solely the component outgoing from the slab. Second, the mode must be evanescent outside the slab. The former requires the amplitudes of incoming waves to vanish, i.e., $B_L^+ = 0$ and $B_R^- = 0$ in Eq. (24). The latter can happen for sufficiently great wave number $k_z > k_0\sqrt{\varepsilon_b}$ in agreement with constitutive Eq. (6), where the x projection k_b of the wave vector and, consequently, the phase shift φ_b become imaginary, see Eqs. (8) and (16). Therefore, the transfer relation (24) gets the form

$$\begin{pmatrix} B_R^+ \\ 0 \end{pmatrix} = \begin{pmatrix} \mathcal{D}_{11} & \mathcal{D}_{12} \\ \mathcal{D}_{21} & \mathcal{D}_{22} \end{pmatrix}\begin{pmatrix} 0 \\ B_L^- \end{pmatrix}. \tag{25}$$

One can readily recognize that the nontrivial solution $B_R^+ = \mathcal{D}_{12}B_L^-$ to this matrix equation exists if and only if the indispensable condition holds true. Specifically,

$$\mathcal{D}_{22} = 0. \tag{26a}$$

With the use of Eq. (8) and Eqs. (18)–(20), the requirement (26a) can be explicitly rewritten as

$$\cot(k_c d_c) = \frac{1}{2}\left[\frac{k_c\varepsilon_b}{\kappa_b\varepsilon_{zz}} - \frac{\kappa_b\varepsilon_{zz}}{k_c\varepsilon_b}\right]. \tag{26b}$$

Thus, the electromagnetic eigenmodes localized on the c slab of layered superconductor exist only when the wave frequency ω and the wave number k_z turn out to be connected by the dispersion relation (26). This dispersion relation was analyzed in detail in Ref. [31]. Here we present the outline of this analysis in order to highlight the features affecting the resonant transmission phenomenon.

Figure 3 shows the family of the dispersion (spectral) curves $\Omega = \Omega_n(k_z)$ of the localized electromagnetic modes obeying Eq. (26b) and enumerated by the integer $n = 0,1,2,3,\ldots$. The dimensionless parameter $\Omega = \omega/\omega_J$ is the wave frequency normalized to the Josephson plasma frequency ω_J. As one can see, all the spectral curves are found to the right from the light line $\Omega = ck_z/\omega_J\sqrt{\varepsilon_b}$ so that the obligatory condition $k_z > k_0\sqrt{\varepsilon_b}$ contained in constitutive Eq. (6) is fulfilled automatically.

The lowest dashed red curve describing the zero-mode spectrum $\Omega = \Omega_0(k_z)$, starts at the coordinate origin $(k_z = 0, \Omega = 0)$ and monotonically increases approaching $\Omega = 1$ as $k_z \to \infty$. Since this curve is wholly located at $\Omega < 1$, the propagation wave number k_c is imaginary according to definition (10) and its subsequent analysis. Thus, the localized mode supported by the lowest dispersion curve $\Omega = \Omega_0(k_z)$ represents a surface wave decaying into the c slab of the layered superconductor.

The behavior of the next dispersion curve $\Omega = \Omega_1(k_z)$ is determined by the thickness d_c of the c slab. In the case $d_c \gtrsim$

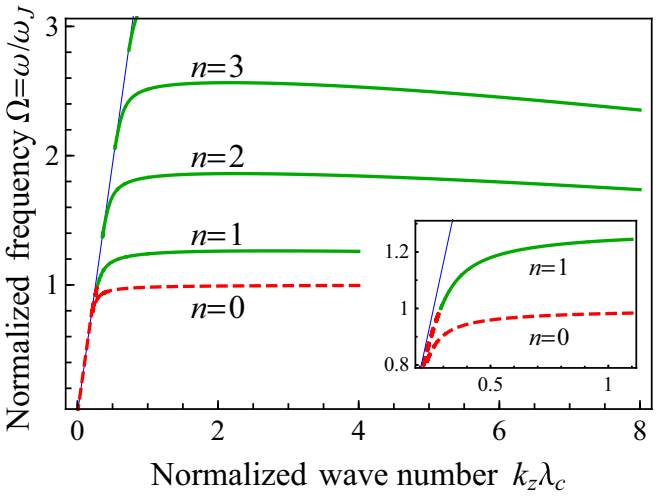

FIG. 3. The normalized wave frequency Ω vs the dimensionless wave number $k_z\lambda_c$ for the localized modes, Eq. (26b). The dashed red curves correspond to the surface modes at $\Omega < 1$ with indices $n = 0,1$, and the solid green curves correspond to the waveguide modes with $n = 1,2,3,\ldots$ at $\Omega = \omega/\omega_J > 1$. The thin blue straight line is the light line, $\Omega = ck_z/\omega_J\sqrt{\varepsilon_b}$. The inset shows the dispersion curves for surface waves and the waveguide modes with $n = 0$ and $n = 1$ in the narrow range near $\Omega = 1$. Parameters: $\varepsilon_b = 1$, $\varepsilon_c = 15$, $d_c/\lambda_c = 1$, $\gamma = \lambda_c/\lambda_{ab} = 15$.

$\lambda_c\gamma\varepsilon_c/\varepsilon_b$, the curve $\Omega = \Omega_1(k_z)$, similarly to $\Omega = \Omega_0(k_z)$, is confined to the interval $0 \leqslant \Omega < 1$ in spite of its monotonic increase and, consequently, describes the spectrum of the surface wave. Figure 3 demonstrates the opposite case of relatively thin c slab with $d_c \ll \lambda_c\gamma\varepsilon_c/\varepsilon_b$. Here the dispersion curve $\Omega = \Omega_1(k_z)$ consists of two parts. The first one with imaginary k_c (the dashed red part) starts at the point ($k_z = 0, \Omega = 0$) and grows up holding $\Omega < 1$. This part corresponds to the surface wave. At $\Omega = 1$ the wave number $k_c = 0$, and the surface wave transforms into the waveguide mode. Indeed, the second, solid green, part of the curve $\Omega = \Omega_1(k_z)$ is located at $\Omega > 1$. As a result, k_c becomes real that implies oscillating character of the electromagnetic field inside the c slab. It is important to note that in this case the dispersion curve $\Omega = \Omega_1(k_z)$ is nonmonotonic because the normalized wave frequency $\Omega \to 1$ from above as $k_z \to \infty$.

All the other solid green dispersion curves $\Omega = \Omega_n(k_z)$ with $n = 2,3,\ldots$ belong to the waveguide modes being completely contained within the frequency interval $\Omega > 1$ and, consequently, providing for the propagation wave number k_c to be real. They start from the threshold,

$$k_z = \frac{\widetilde{\Omega}_n}{c}\omega_J\sqrt{\varepsilon_b}, \quad \Omega = \widetilde{\Omega}_n \equiv \sqrt{1 + [\pi(n-1)\lambda_c/d_c]^2}, \tag{27a}$$

located on the light line $\Omega = ck_z/\omega_J\sqrt{\varepsilon_b}$. After the threshold, the nth dispersion curve $\Omega = \Omega_n(k_z)$ increases with increasing k_z, achieves its maximum $\Omega = \Omega_n^{(\max)}$ and then begins to decrease. Sufficiently far from the threshold, the nth curve decreases as

$$\Omega_n(k_z) \approx \sqrt{1 + \frac{(\pi n\lambda_c/d_c)^2}{1 + (k_z\lambda_{ab})^2}} \tag{27b}$$

and tends from above to the limit $\Omega = 1$ when $k_z \to \infty$.

In summary, the dispersion curves $\Omega = \Omega_n(k_z)$ with $n = 1,2,3,\ldots$ are nonmonotonic consisting of two parts. The first, growing up, part corresponds to the nth localized mode with normal dispersion, i.e., both velocities, the phase one, Ω_n/k_z, and the group one, $d\Omega_n/dk_z$, have the positive sign. The second, falling down, part describes the same nth mode, however, with anomalous dispersion where the phase and the group velocities are of opposite signs. This peculiar property of the spectrum $\Omega = \Omega_n(k_z)$ governed by the dispersion relation (26) gives rise to a nontrivial dependence of the transmittance T on the incidence angle θ analyzed in Sec. VI. Indeed, for a certain value of the dimensionless wave frequency $\Omega > 1$, there can be found two values of the wave number k_z which provide the excitation of the nth waveguide mode localized inside the c slab. As a consequence, two resonant peaks should appear in the $T(\theta)$ dependence. Moreover, when approaching the maximum of $\Omega = \Omega_n(k_z)$ for the nth mode, these peaks should merge turning into the substantially broadened single peak.

It should be emphasized that the existence of the nonmonotonic spectral curves $\Omega = \Omega_n(k_z)$ for the localized modes is an inherent property of hyperbolic media since it directly originates from the different signs of the components of the effective permittivity tensor; see the discussion in the end of Sec. II. The layered superconductors, belonging to such media, can serve as promising objects for the observation and study of the considered phenomena in a wide THz frequency range.

V. UNILATERAL EXCITATION

The knowledge of the explicit expressions (22) for the elements of the total transfer matrix $\hat{M}^{(T)}$ allows one to obtain the transmittance T of the setup under consideration, see Fig. 1. By definition [33],

$$T = \left|M_{22}^{(T)}\right|^{-2} = \left[1 + M_{12}^{(T)}M_{21}^{(T)} + M_{22}^{(T)}\left(M_{22}^{(T)*} - M_{11}^{(T)}\right)\right]^{-1}. \tag{28}$$

The second line of Eq. (28) directly follows from the unimodularity condition (21b), with the asterisk "$*$" standing for complex conjugation.

To proceed further analytically, we suppose the absence of dissipation in the layered superconductor, i.e., the dimensionless relaxation frequencies are regarded to vanish in Eqs. (9), $\nu_x = 0$ and $\nu_z = 0$. Later on, we shall present the effect of dissipation with corresponding numerical simulations, see Sec. VII.

Without dissipation, the frequency-dispersive permittivity tensor (9) of the c slab is real valued. As a consequence, the total transfer matrix $\hat{M}^{(T)}$ meets the time-reversal symmetry,

$$M_{22}^{(T)} = M_{11}^{(T)*}, \quad M_{21}^{(T)} = M_{12}^{(T)*}. \tag{29}$$

Indeed, the parameters κ_b, ϕ_b, and $\beta_\pm$ in Eqs. (22) take real values, see, respectively, Eqs. (8), (16), and (23b). At the same

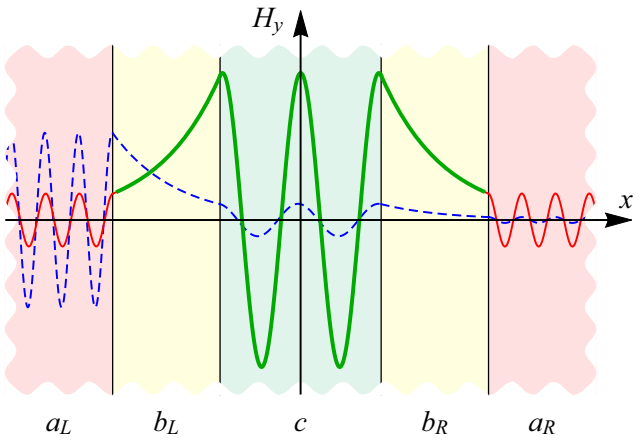

FIG. 4. The principal distribution of the magnetic field in the wave transferred through the system. The thick solid line in the b_L-c-b_R subsystem represents the exited localized mode causing the resonant transmission.

time, k_c along with φ_c and $\alpha_\pm$ can be either real or imaginary. However, the product $\alpha_\pm \sin\varphi_c$ and $\cos\varphi_c$ are always real. The transfer matrix $\hat{\mathcal{D}}$ for the c slab is real valued and does not obey the time-reversal symmetry (29). In spite of this fact, the total transfer matrix $\hat{M}^{(T)}$ is symmetrical with respect to the time-reversal operation, Eq. (29).

Due to symmetry (29), the general expression (28) for the transmittance T is simplified to the form appropriate for the subsequent analysis,

$$T = \frac{1}{1 + M_{12}^{(T)} M_{21}^{(T)}} = \{1 + [\beta_- \sinh 2\phi_b \cos\varphi_c + (\beta_-\alpha_+ \cosh 2\phi_b + \beta_+\alpha_-)\sin\varphi_c]^2\}^{-1}. \quad (30)$$

Thus, the optic transmission of the system obeying the time-reversal symmetry is completely specified by off-diagonal elements of its total transfer matrix. One should also emphasize that, in line with the time-reversal symmetry (29), the expression in the square brackets of Eq. (30) is always real valued. Consequently, the transmittance T should be smaller than or equal to one, $T \leqslant 1$. The equality $T = 1$ is achieved only for such values of parameters, when the expression placed inside the square brackets vanishes.

VI. RESONANT TRANSMISSION DUE TO EXCITATION OF LOCALIZED MODES: ANOMALOUS DISPERSION

The main interest in the analysis of transmittance (30) under conditions (6) is due to the resonant character of the $T(\theta)$ dependence caused by the excitation of localized modes. Figure 4 presents the principal distribution of the magnetic field in the wave transferred through the system. The dashed line is plotted for the regular transmission, when the electromagnetic field is decreasing while the wave passes the spatial b gaps. This causes the transmittance to be exponentially small. On the contrary, the solid line shows the resonant transmission, when the electromagnetic field in the spatial b gaps can increase and the localized mode (see the thick solid line in the b_L-c-b_R subsystem) can be exited. In the last case, the transmittance can be significantly enhanced up to 1.

This phenomenon is clearly pronounced if the spatial b gaps are sufficiently thick, i.e., when the modulus ϕ_b of the phase shift φ_b is large, see Eq. (16),

$$\exp(-2\phi_b) \ll |\exp(i\varphi_c)|. \quad (31a)$$

In this case the right-hand side of the inequality (31a) equals one when the phase shift φ_c is real and is smaller than one in the opposite case of imaginary φ_c. Thus, $\exp(-2\phi_b)$ should be much smaller than one in both cases. This fact allows us to replace $\sinh(2\phi_b)$ and $\cosh(2\phi_b)$ in Eq. (30) with $\exp(2\phi_b)/2$ and, as a result, to arrive at the following asymptotics for the transmittance

$$T = \left[1 + \tfrac{1}{4}(\beta_-\mathcal{D}_{22}\exp(2\phi_b) + 2\beta_+\alpha_-\sin\varphi_c)^2\right]^{-1}. \quad (31b)$$

Far from the resonance, where

$$|\mathcal{D}_{22}| \equiv |\cos\varphi_c + \alpha_+ \sin\varphi_c| \gg \exp(-2\phi_b), \quad (32a)$$

the transmission is exponentially suppressed because of strong wave attenuation within the spatial b gaps,

$$T = \frac{4\exp(-4\phi_b)}{\beta_-^2\mathcal{D}_{22}^2}. \quad (32b)$$

However, for certain values of the problem parameters, the transmission can be significantly enhanced. Indeed, if the frequency ω and the incidence angle θ nearly satisfy the dispersion relation (26) for the localized modes,

$$|\mathcal{D}_{22}| \equiv |\cos\varphi_c + \alpha_+ \sin\varphi_c| \lesssim \exp(-2\phi_b) \ll 1, \quad (33)$$

then the term $\mathcal{D}_{22}\exp(2\phi_b)$ is not exponentially great, and the transmittance is not exponentially small. Moreover, when

$$\mathcal{D}_{22} = -2\beta_-^{-1}\beta_+\alpha_- \sin\varphi_c \exp(-2\phi_b), \quad (34)$$

the round-bracketed expression in Eq. (31b) vanishes, and the perfect transmission with $T = 1$ occurs.

Figure 5 presents the transmittance T as a function of the incidence angle θ and the normalized frequency $\Omega = \omega/\omega_J$. Here, the darker color corresponds to the greater value of T. The dispersion curves $\Omega = \Omega_n(\theta)$ for the localized modes, governed by Eqs. (26), are also plotted in the solid green. Since our setup includes the connecting a leads, the spectral curves are properly regarded as functions of the incidence angle θ instead of the wave number k_z in agreement with definition (4). Therefore, the light line $\Omega = ck_z/\omega_J\sqrt{\varepsilon_b}$ in Fig. 3 restricting from the left the definitional domain of the mode spectrum turns into the vertical straight line $\theta = \theta_b$ in Fig. 5. In addition, there appears the upper limit for θ equal to $\pi/2$. In other words, the left condition in Eq. (6) confining the wave number k_z is reformulated into the right one for the incidence angle θ. It is noteworthy, within the constitutive range (6), each of the spectral curves $\Omega = \Omega_n(\theta)$ with indices $n \geqslant 2$ in Fig. 5 occupies its own frequency domain (spectral band) on the (θ,Ω) phase plane, separated from the frequency bands of two adjacent (neighboring) dispersion curves with indices $n-1$ and $n+1$ by the corresponding spectral (frequency) gaps with exponentially small transmission.

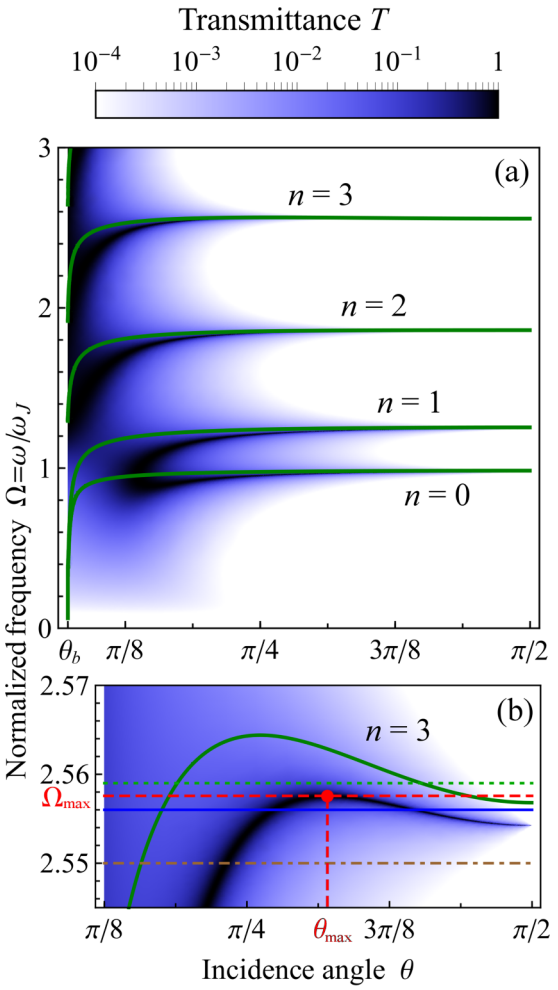

FIG. 5. Transmittance T vs the incidence angle θ and the normalized frequency $\Omega = \omega/\omega_J$. The solid green lines represent the dispersion curves for the localized modes in the system with infinite thicknesses of the spatial b gaps, see Eqs. (26) and Fig. 3. Panel (b) shows the region around the maximum in the dispersion curve with $n = 3$. Four horizontal straight lines in panel (b) correspond to the values of Ω used in Fig. 6. The solid red circle marks the top point $\theta_{max} = 1.0057$ and $\Omega_{max} = 2.5576$ on the dispersion curve for setup with finite d_b, Eq. (34). Parameters: $\varepsilon_a = 20$, $d_b/\lambda_c = 1/7$. The other parameters are the same as in Fig. 3.

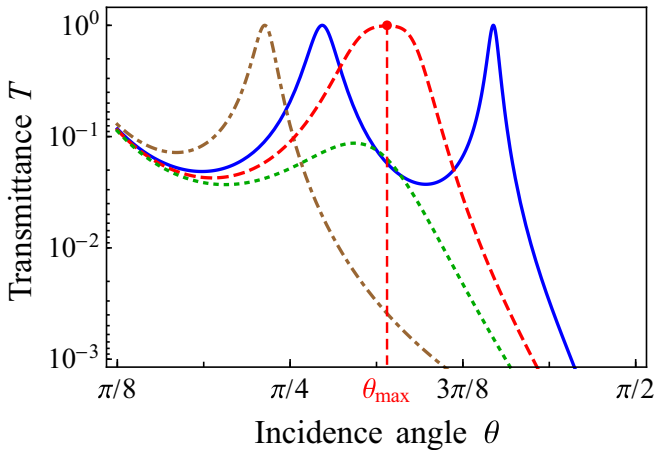

FIG. 6. Transmittance T vs the incidence angle θ for four values of the normalized frequency: $\Omega = 2.55$ (dot-dashed brown curve), $\Omega = 2.556$ (solid blue curve), $\Omega = \Omega_{max} = 2.5576$ (dashed red curve), and $\Omega = 2.559$ (dotted green curve). The solid red circle marks the top point $\theta_{max} = 1.0057$ and $T_{max} = 1$ of the broadened peak. The other parameters are the same as in Fig. 5.

One can see that the green dispersion curves resemble the corresponding black areas where $T = 1$, however, deviate from them. The reason for such a deviation consists of a finite value of thickness d_b of the spatial b gaps. While the conventional dispersion relation (26) is obtained for the model with semi-infinite spatial b gaps, in a real setup containing finite constituents, the thickness d_b of the spatial b gaps alters the dispersion relation to the form (34). The discussed deviation is reduced by increasing the phase shift ϕ_b, specifically, with increase of the thickness d_b or the incidence angle θ, see Eq. (16). Evidently, both relations, (26) and (34), coincide as $d_b \to \infty$. Thus, Eq. (31b) and Fig. 5 elucidate that the resonant perfect transmission with $T = 1$ is induced by excitation of the specific electromagnetic modes localized on the c slab of layered superconductor, however, with modified spectrum obeying the dispersion relation (34). Remarkably, the perturbed by d_b dispersion curves $\Omega = \Omega_n(\theta)$ keep all the main peculiarities of the unperturbed curves despite the perceptible quantitative difference. In what follows, in order to avoid introducing new notations, $\Omega = \Omega_n(\theta)$ shall be refereed to as the real-valued solution of the new perturbed dispersion equation (34).

The inherent peculiarity of the resonant transmission through the system containing a layered superconductor is the nonmonotony of the dispersion law for the localized modes: Each dispersion curve consists of two parts, with normal, $d\Omega_n/d\theta > 0$, and anomalous, $d\Omega_n/d\theta < 0$, dispersion that is clearly displayed in the panel (b) of Fig. 5. Note, according to definition (4), the sign of the derivative $d\Omega_n/d\theta$ coincides with the sign of the group velocity $d\omega/dk_z$ of the localized mode. Therefore, the concept of the normal and anomalous dispersion used here is equivalent to that introduced in Sec. IV.

The dynamics of the resonance line shape in the $T(\theta)$ dependence provided by the nonmonotony of the spectral curves is illustrated in Fig. 6. One can see four $T(\theta)$ curves depicted for four close values of the normalized frequency Ω. For the lowest frequency $\Omega = 2.55$, there is just a single, normally dispersive, solution $\theta = \theta^{(+)}(\Omega)$ of the dispersion relation (34) that is located on the growing part of the dispersion curve [see panel (b) in Fig. 5]. This solution corresponds to the single, relatively narrow, resonant peak with $T = 1$ of the dot-dashed brown line $T(\theta)$. At $\Omega = 2.556$, in addition to the solution $\theta = \theta^{(+)}(\Omega)$ with normal dispersion there arise the second, anomalously dispersive, solution $\theta = \theta^{(-)}(\Omega)$ that belongs to the falling down part of the spectral curve. As a result, the solid blue curve $T(\theta)$ contains two resonant peaks with perfect transmission. When the normalized frequency attains to the value $\Omega = \Omega_{max}$ where the dispersion curve achieves its maximum denoted with the solid red circle in panel (b) of Fig. 5, the twin peaks degenerate into the single broad one with $T = 1$ as shown by the dashed red curve in Fig. 6. In agreement with the dotted green straight line presented in

panel (b) of Fig. 5, the normalized frequency $\Omega = 2.559$ gets inside the spectral gap where the solution $\theta = \theta(\Omega)$ to the perturbed dispersion relation (34) turns out to be of complex value. Therefore, the $T(\theta)$ dependence described by the dotted green curve in Fig. 6, being exponentially suppressed ($T \ll 1$), does not experience the resonant excitation of the localized mode.

In order to clarify analytically the dynamics of the resonant peaks in the dependence of $T(\theta)$, we perform below the general study of its line shape for two different cases, when the frequency Ω is far from or close to the maximum frequency $\Omega_{\max}$ marked on the perturbed dispersion curve in panel (b) of Fig. 5.

A. Resonance line shape for Ω far from $\Omega_{\max}$

The perfect transmission with $T = 1$ occurs when the spectral function

$$\rho(\theta,\Omega) \equiv \tfrac{1}{2}\beta_{-}\mathcal{D}_{22}\exp(2\phi_b) + \beta_{+}\alpha_{-}\sin\varphi_c \tag{35a}$$

entering the expression (31b) for the transmittance T, vanishes,

$$\rho(\theta,\Omega) = 0, \tag{35b}$$

at certain real value $\theta = \theta_0$ of the incidence angle and corresponding resonant (real) value $\Omega = \Omega_0 \equiv \Omega_n(\theta_0)$ of the normalized frequency, where the nth localized mode is excited.

Consider the point (θ_0,Ω_0) to be located on the left, growing, normally dispersive part of the spectral curve $\Omega = \Omega_n(\theta)$, far from the top point $(\theta_{\max},\Omega_{\max})$. In this case, the expansion of the spectral function $\rho(\theta,\Omega)$ in small deviations from θ_0 and Ω_0 can be restricted by linear approximation,

$$\rho(\theta,\Omega) = \left[\frac{\partial\rho}{\partial\theta}\right]_0(\theta-\theta_0) + \left[\frac{\partial\rho}{\partial\Omega}\right]_0(\Omega-\Omega_0). \tag{36}$$

Here the symbol $[\ldots]_0$ means substituting the values $\theta = \theta_0$ and $\Omega = \Omega_0$ into the inner expression. With the use of this expansion, Eq. (31b) for the transmittance $T(\theta)$ is reduced to the conventional Lorentzian form

$$T(\theta) = \frac{\Theta_{\text{norm}}^2}{\Theta_{\text{norm}}^2 + (\theta-\theta_{\text{peak}})^2}. \tag{37a}$$

The position $\theta = \theta_{\text{peak}}$ of the only resonant peak with $T(\theta_{\text{peak}}) = 1$ is determined by

$$\theta_{\text{peak}} = \theta_0 + \left[\frac{d\Omega_n}{d\theta}\right]_0^{-1}(\Omega-\Omega_0), \tag{37b}$$

and its half-width Θ_{norm} turns out to be proportional to $\exp(-2\phi_b)$,

$$\Theta_{\text{norm}} = \left|\frac{\partial\rho}{\partial\theta}\right|_0^{-1} \propto \exp(-2\phi_b). \tag{37c}$$

Note that the derivative

$$\left[\frac{d\Omega_n}{d\theta}\right]_0 = -\left[\frac{\partial\rho}{\partial\theta}\Big/\frac{\partial\rho}{\partial\Omega}\right]_0 \tag{38}$$

should be positive by definition of the normal dispersion.

In accordance with Eq. (16), increasing the spatial b gap thickness d_b or the incidence angle θ results in the increase of the phase-shift modulus ϕ_b, and, as a consequence of Eq. (37c), in the thinning of the resonant peak. An example of the $T(\theta)$ dependence described by Eqs. (37) is given by the dot-dashed brown curve in Fig. 6.

B. Resonance line shape for Ω close to $\Omega_{\max}$

As the dispersion curve $\Omega = \Omega_n(\theta)$ defined by Eqs. (35) is nonmonotonic, it achieves the top (maximum) point $\Omega_{\max} = \Omega_n(\theta_{\max})$ in which the following conditions are met:

$$\rho(\theta_{\max},\Omega_{\max}) = 0, \quad \left[\frac{\partial\rho}{\partial\theta}\right]_{\max} = -\left[\frac{\partial\rho}{\partial\Omega}\frac{d\Omega_n}{d\theta}\right]_{\max} = 0, \tag{39a}$$

with the notation $[\ldots]_{\max}$ implying the value of the inner expression taken at $\theta = \theta_{\max}$ and $\Omega = \Omega_{\max}$. Therefore, the expansion of the spectral function $\rho(\theta,\Omega)$ in the vicinity of the top point should be extended up to the quadratic approximation in the deviation $\theta - \theta_{\max}$,

$$\rho(\theta,\Omega) = \left[\frac{\partial^2\rho}{\partial\theta^2}\right]_{\max}(\theta-\theta_{\max})^2 + \left[\frac{\partial\rho}{\partial\Omega}\right]_{\max}(\Omega-\Omega_{\max}). \tag{39b}$$

This expansion gives rise to the following expression for the transmittance $T(\theta)$:

$$T(\theta) = \frac{\Theta_{\text{anom}}^4}{\Theta_{\text{anom}}^4 + \left[(\theta-\theta_{\max})^2 - \delta\theta_{\text{peak}}^2\right]^2}. \tag{40a}$$

Here the squared resonant θ shift read

$$\delta\theta_{\text{peak}}^2 = \left[\frac{d^2\Omega_n}{d\theta^2}\right]_{\max}^{-1}(\Omega-\Omega_{\max}), \tag{40b}$$

and the parameter of the resonance-line width is referred to as

$$\Theta_{\text{anom}} = \left|\frac{\partial^2\rho}{\partial\theta^2}\right|_{\max}^{-1/2} \propto \exp(-\phi_b). \tag{40c}$$

At the maximum point $(\theta_{\max},\Omega_{\max})$, the second derivative of the spectrum $\Omega = \Omega_n(\theta)$ is negative and can be associated with the corresponding derivatives of the spectral function $\rho(\theta,\Omega)$,

$$\left[\frac{d^2\Omega_n}{d\theta^2}\right]_{\max} = -\left[\frac{\partial^2\rho}{\partial\theta^2}\Big/\frac{\partial\rho}{\partial\Omega}\right]_{\max} < 0. \tag{41}$$

For fixed frequency $\Omega < \Omega_{\max}$, the parameter $\delta\theta_{\text{peak}}^2$ is positive, $\delta\theta_{\text{peak}}^2 > 0$. As a consequence, Eq. (40a) describes two close peaks positioned at the points $\theta = \theta_{\text{peak}} \equiv \theta_{\max} \pm \delta\theta_{\text{peak}}$ with $T(\theta_{\text{peak}}) = 1$. The line shape of $T(\theta)$ dependence near all of the twin peaks is Lorentzian,

$$T(\theta) = \frac{\Theta_{\text{twin}}^2}{\Theta_{\text{twin}}^2 + (\theta-\theta_{\max}\pm\delta\theta_{\text{peak}})^2}, \quad \Omega < \Omega_{\max}, \tag{42a}$$

with the half-width Θ_{twin} being determined by

$$\Theta_{\text{twin}} = \Theta_{\text{anom}}^2/2\delta\theta_{\text{peak}} \propto \exp(-2\phi_b). \tag{42b}$$

Such a situation emerges due to the coexistence of normal and anomalous dispersions in the frequency spectrum $\Omega = \Omega_n(\theta)$. It is displayed by the solid blue curve in Fig. 6.

When the normalized frequency $\Omega = \Omega_{\max}$, the parameter $\delta\theta_{\text{peak}}^2$ vanishes, $\delta\theta_{\text{peak}} = 0$. Hence, two previous peaks

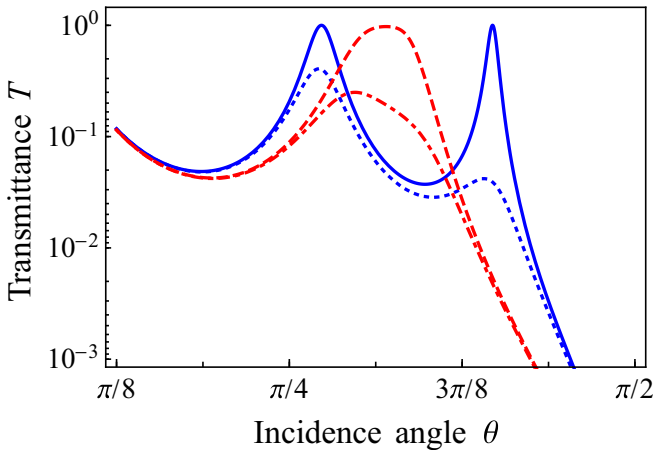

FIG. 7. Transmittance T vs the incidence angle θ for two values of the normalized frequency, $\Omega = 2.556$ and $\Omega = \Omega_{\max} = 2.5576$: respectively, solid blue and dashed red curves related to $\nu_x = \nu_z = 0$, and dotted blue and dot-dashed red curves associated with $\nu_x = \nu_z = 10^{-3}$. The other parameters are the same as in Fig. 6.

merge into the single broad one positioned at $\theta_{\text{peak}} = \theta_{\max}$ with $T(\theta_{\max}) = 1$. The $T(\theta)$ dependence is described by the degenerated line shape,

$$T(\theta) = \frac{\Theta_{\text{anom}}^4}{\Theta_{\text{anom}}^4 + (\theta - \theta_{\max})^4}. \tag{43}$$

This expression is illustrated by the dashed red curve in Fig. 6. The parameter Θ_{anom} defining the half-width of the peak, is proportional to $\exp(-\phi_b)$. Consequently, the width of the single broad peak appears to be in $\exp(\phi_b) \gg 1$ times greater than the width of the single normal peak governed by Eqs. (37), as well as the width of each of the twin peaks obeying Eqs. (42).

Finally, for certain $\Omega > \Omega_{\max}$, which is located inside the spectral gap, the parameter $\delta\theta_{\text{peak}}^2$ expectedly becomes negative, $\delta\theta_{\text{peak}}^2 < 0$, and the resonant θ-shift $\delta\theta_{\text{peak}}$ turns out to be imaginary. Equation (40a) shows that there is no resonance in this case since the excitation of the localized mode is absent in the spectral gap. The $T(\theta)$ dependence may contain the only peak, very weak and broad, with $T_{\max} \ll 1$ situated at $\theta_{\text{peak}} = \theta_{\max}$ and arising due to proximity to the resonance at the top point $\Omega = \Omega_{\max}$ of the dispersion curve, see dotted green curve in Fig. 6.

VII. RESONANT TRANSMISSION WITH ACCOUNT FOR DISSIPATION

All results obtained in Sec. VI are valid for the case of negligible dissipation, $\nu_x = 0$ and $\nu_z = 0$, in the c slab of the layered superconductor. However, even in the case of finite dissipation the most important features of the resonant transmission caused by the excitation of the localized modes can be observed. To demonstrate this fact we have realized the numerical calculations of transmittance T based on its general definition (28) complemented by expression (22d) for the element $M_{22}^{(T)}$ of the total transfer matrix. The corresponding results are plotted in Fig. 7.

The solid blue line ($\Omega = 2.556$) and dashed red line ($\Omega = \Omega_{\max} = 2.5576$) which are obtained for $\nu_x = \nu_z = 0$ and taken from Fig. 6, show two close peaks and a single broadened peak in the $T(\theta)$ dependence, respectively. The dotted blue line and dot-dashed red line are depicted for the same corresponding values of the dimensionless frequency Ω, however, for nonzero $\nu_x = 10^{-3}$ and $\nu_z = 10^{-3}$. One can see that the two close peaks and single broadened peak persist even in the case of small (but realistic) dissipation.

VIII. CONCLUSIONS

We have presented the theoretical study of the THz wave transmission through a slab of layered superconductor separated from two dielectric leads by spatial gaps made from a dielectric material of softer optical density. Using the transfer matrix techniques, we have derived the analytic expression for the transmittance T and have analyzed it in detail as a function of the angle θ of the wave incidence from the lead onto the lead-gap interface. We have determined the conditions for the perfect transmission with $T = 1$ and revealed the possibility of excitation of the specific electromagnetic modes localized on the layered superconductor. Such modes occur when the wave does not propagate inside the spatial gaps resulting in strong resonant enhancement of the transmission. The inherent features of this phenomenon are directly related to the nontrivial electrodynamics of the Josephson plasma in the layered superconductor, which represents a hyperbolic medium in a wide range of the THz frequencies. The nonmonotony of the dispersion law $\omega = \omega(\theta)$ for the localized modes gives rise to emerging two resonant peaks in the $T(\theta)$ dependence associated with the same value of the wave frequency ω and their merge into the broadened single peak with subsequent ω increase.

It is important to emphasize that the phenomena predicted here can be fine tuned by a weak external DC magnetic field, similarly to what happens with the other electromagnetic effects in the layered superconductors (see, e.g., Ref. [34]). This opens prospects for possible future applications, such as tuning the emission or receiver frequency from THz sources.

ACKNOWLEDGMENTS

We gratefully acknowledge partial support from the grant of State Fund For Fundamental Research of Ukraine (Project No. Ф76/33683) and from the CONACYT (México).

[1] V. G. Veselago, Sov. Phys. Usp. **10**, 509 (1968).
[2] J. B. Pendry and D. R. Smith, Phys. Today **57**, 37 (2004).
[3] K. Y. Bliokh, Y. P. Bliokh, V. Freilikher, S. Savel'ev, and F. Nori, Rev. Mod. Phys. **80**, 1201 (2008).
[4] J. B. Pendry, Phys. Rev. Lett. **85**, 3966 (2000).

[5] L. I. Mandelstam, Zh. Eksp. Teor. Fiz. **15**, 475 (1945); [in Russian].
[6] V. M. Shalaev, Nat. Photonics **1**, 41 (2007).
[7] R. A. Shelby, D. R. Smith, and S. Schultz, Science **292**, 77 (2001).
[8] V. A. Podolskiy and E. E. Narimanov, Phys. Rev. B **71**, 201101(R) (2005).
[9] J. B. Pendry, Science **306**, 1353 (2004).
[10] A. Alu and N. Engheda, J. Opt. Soc. Am. B **23**, 571 (2006).
[11] O. V. Ivanov and D. I. Sementsov, Crystallogr. Rep. **45**, 487 (2000).
[12] A. L. Rakhmanov, V. A. Yampol'skii, J. A. Fan, F. Capasso, and F. Nori, Phys. Rev. B **81**, 075101 (2010).
[13] V. A. Golick, D. V. Kadygrob, V. A. Yampol'skii, A. L. Rakhmanov, B. A. Ivanov, and F. Nori, Phys. Rev. Lett. **104**, 187003 (2010).
[14] S. Savel'ev, V. Yampol'skii, and F. Nori, Phys. Rev. Lett. **95**, 187002 (2005).
[15] V. A. Yampol'skii, D. R. Gulevich, S. Savel'ev, and F. Nori, Phys. Rev. B **78**, 054502 (2008).
[16] R. Kleiner, F. Steinmeyer, G. Kunkel, and P. Muller, Phys. Rev. Lett. **68**, 2394 (1992).
[17] R. Kleiner and P. Muller, Phys. Rev. B **49**, 1327 (1994).
[18] S. Savel'ev, V. A. Yampol'skii, A. L. Rakhmanov, and F. Nori, Rep. Prog. Phys. **73**, 026501 (2010).
[19] X. Hu and S.-Z. Lin, Supercond. Sci. Technol. **23**, 053001 (2010).
[20] O. K. C. Tsui, N. P. Ong, Y. Matsuda, Y. F. Yan, and J. B. Peterson, Phys. Rev. Lett. **73**, 724 (1994).
[21] M. Palumbo and M. J. Graf, Phys. Rev. B **53**, 2261 (1996).
[22] A. A. Koulakov and A. I. Larkin, Phys. Rev. B **59**, 12021 (1999).
[23] Yu. I. Latyshev, A. E. Koshelev, and L. N. Bulaevskii, Phys. Rev. B **68**, 134504 (2003).
[24] U. Welp, K. Kadowaki, and R. Kleiner, Nat. Photon. **7**, 702 (2013).
[25] K. Nakade, T. Kashiwagi, Y. Saiwai, H. Minami, T. Yamamoto, R. A. Klemm, and K. Kadowaki, Sci. Rep. **6**, 23178 (2016).
[26] I. Kakeya and H. Wang, Supercond. Sci. Technol. **29**, 073001 (2016).
[27] T. Kashiwagi, H. Kubo, K. Sakamoto, T. Yuasa, Y. Tanabe, C. Watanabe, T. Tanaka, Y. Komori, R. Ota, G. Kuwano, K. Nakamura, T. Katsuragawa, M. Tsujimoto, T. Yamamoto, R. Yoshizaki, H. Minami, K. Kadowaki, and R. A. Klemm, Supercond. Sci. Technol. **30**, 074008 (2017).
[28] T. Kashiwagi, K. Sakamoto, H. Kubo, Y. Shibano, T. Enomoto, T. Kitamura, K. Asanuma, T. Yasui, Ch. Watanabe, K. Nakade, Y. Saiwai, T. Katsuragawa, M. Tsujimoto, R. Yoshizaki, T. Yamamoto, H. Minami, R. A. Klemm, and K. Kadowaki, Appl. Phys. Lett. **107**, 082601 (2015).
[29] E. A. Borodiansky and V. M. Krasnov, Nat. Commun. **8**, 1742 (2017).
[30] T. M. Slipchenko, D. V. Kadygrob, D. Bogdanis, V. A. Yampol'skii, and A. A. Krokhin, Phys. Rev. B **84**, 224512 (2011).
[31] S. S. Apostolov, V. I. Havrilenko, Z. A. Maizelis, and V. A. Yampol'skii, Low Temp. Phys. **43**, 296 (2017).
[32] F. M. Izrailev, A. A. Krokhin, and N. M. Makarov, Phys. Rep. **512**, 125 (2012).
[33] P. Markoš and C. M. Soukoulis, *Wave Propagation: From Electrons to Photonic Crystals and Left-Handed Materials* (Princeton University Press, Princeton, 2008), p. 376.
[34] S. S. Apostolov, Z. A. Maizelis, N. M. Makarov, F. Pérez-Rodríguez, T. N. Rokhmanova, and V. A. Yampol'skii, Phys. Rev. B **94**, 024513 (2016).